Arrays of nanoscale magnetic dots: Fabrication by x-ray interference lithography and characterization

L. J. Heyderman,[a] H. H. Solak, and C. David
Laboratory for Micro- and Nanotechnology, Paul Scherrer Institut, CH-5232 Villigen PSI, Switzerland

D. Atkinson and R. P. Cowburn
Nanomagnetism Group, Department of Physics, University of Durham, Rochester Building, Science Laboratories, South Road, Durham DH1 3LE, United Kingdom

F. Nolting
Swiss Light Source, Paul Scherrer Institut, CH-5232 Villigen PSI, Switzerland

(Received 9 June 2004; accepted 20 September 2004)

X-ray interference lithography (XIL) was employed in combination with electrodeposition to fabricate arrays of nanoscale nickel dots which are uniform over 40 μm and have periods down to 71 nm. Using extreme-ultraviolet light, XIL has the potential to produce magnetic dot arrays over large areas with periods well below 50 nm, and down to a theoretical limit of 6.5 nm for a 13 nm x-ray wavelength. In the nickel dot arrays, we observed the effect of interdot magnetic stray field interactions. Measuring the hysteresis loops using the magneto-optical Kerr effect, a double switching via the vortex state was observed in the nickel dots with diameters down to 44 nm and large dot separations. As the dot separations are reduced to below around 50 nm a single switching, occurring by collective rotation of the magnetic spins, is favored due to interdot magnetic stray field interactions. This results in magnetic flux closure through several dots which could be visualized with micromagnetic simulations. Further evidence of the stray field interactions was seen in photoemission electron microscopy images, where bands of contrast corresponding to chains of coupled dots were observed. © *2004 American Institute of Physics*. [DOI: 10.1063/1.1821649]

It has become increasingly important to find alternatives to current data storage technologies in order to meet the demands for increasing storage capacity. With this aim in mind, there is at present a large effort involved in finding suitable methods for fabricating large area arrays of densely packed, isolated magnetic elements. Such arrays can provide a way to achieve higher areal densities with conventional magnetic recording media[1–3] and are also of interest for use as high density magnetic random access memory cells.[4] In addition, arrays of small ferromagnetic elements provide model systems for magnetic investigations, allowing for example the study of magnetic spin structures, stray field interactions, shape anisotropy, and magnetic switching at the nanoscale. In the present work, we have fabricated nanoscale nickel dot arrays down to periods of 71 nm using x-ray interference lithography (XIL) in combination with electrodeposition. In addition we have studied the magnetic behavior of the dot arrays, investigating the magnetic switching with magneto-optical Kerr effect (MOKE) measurements and carrying out magnetic imaging using photoemission electron microscopy (PEEM). An insight into the observed behavior was obtained using micromagnetic simulations.

First we take a closer look at XIL and show that it has several advantages over other methods available for fabricating magnetic dot arrays. XIL employs extreme-ultraviolet (EUV) light passing through a grating mask to form multiple beams and the resulting interference pattern is exposed in a polymer resist to produce nanoscale periodic structures.[5,6] It is envisaged that with this method, future development of the x-ray masks will allow us to fabricate dot arrays with periods well below 50 nm. A similar interference technique has been employed to manufacture magnetic nanostructures with laser radiation,[7] but the longer laser wavelength, 193 nm compared with 13 nm for EUV light, gives a lower limit to the period of about 100 nm. Compared with electron-beam lithography there is practically no proximity-effect, facilitating the fabrication of dense structures, and the throughput is higher because it is a parallel exposure process. Self-assembly methods for fabricating arrays of magnetic dots or particles[8–10] do not have the specific control of the array geometry achievable with XIL, often requiring templates to achieve long-range ordering. While magnetic particles with sizes of a few nanometers can be fabricated and assembled,[10] XIL has the benefit of being able to pattern any material that can be deposited as a thin film. Focused-ion beam lithography has been used to produce periods down to 56 nm, and writing and reading to the magnetic islands has been demonstrated.[11] However, like electron-beam lithography this is a slow serial patterning method and ion beam damage to the edges of the magnetic element may become critical as the lateral dimensions of the magnetic elements decrease. In comparison with nanoimprint lithography,[1] XIL has the advantage that it is a noncontact lithography, so that surface particle contamination is not critical and there is no mechanical stress applied to the substrate.

To fabricate the nickel dot arrays, we used substrates consisting of 50-nm-thick polymethylmethacrylate resist (molecular weight 600 kg/mol), spin-coated onto an oxidized silicon wafer with a Cr 30 nm/Ge 10 nm sputtered seed layer for electrodeposition.[12] Square arrays of holes were patterned in the resist at the XIL beamline, Swiss Light Source using an XIL mask consisting of Si_3N_4/Cr gratings on a silicon nitride membrane fabricated using electron beam lithography.[5] The hole arrays have periods, p, of 113, 99, 85,

[a]Electronic mail: laura.heyderman@psi.ch

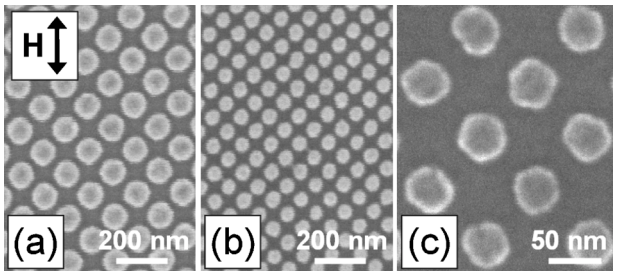

FIG. 1. SEM images of nickel dot arrays fabricated by x-ray interference lithography: (a) $d=95$ nm, $s=18$ nm, $h=40$ nm, (b) $d=55$ nm, $s=16$ nm, $h=40$ nm, and (c) high resolution image showing edge irregularities for $d=44$ nm, $s=27$ nm, $h=16$ nm. The orientation of the applied field, H, for MOKE measurements is indicated by the double headed arrow.

and 71 nm, and array sizes of 50, 57, 67, and 80 μm, respectively. Dot diameters, d, ranging from 40 to 90 nm were achieved by varying the x-ray dose with exposure times ranging between 5 and 35 s depending on the geometry of the grating in the XIL mask. The holes created by XIL are filled with nickel by electrodeposition in a nickel sulphamate bath at a temperature of 50 °C. Typical nickel dot arrays are shown in Figs. 1(a) and 1(b). Detailed inspection using a high resolution SEM of an 80 μm square array of dots with $p=71$ nm [Fig. 1(c)] showed, despite edge irregularities, a uniform dot diameter of $d=(44\pm1.5)$ nm over the central 40 μm square area. The height of the dots was measured using an atomic force microscope to be $h=(16\pm1.5)$ nm. There are changes in the dot size toward the array boundaries due to x-ray diffraction effects which can be removed by suitable masking of the interference pattern during exposure.

Hysteresis loop measurements of the dot arrays were carried out using a high sensitivity MOKE.[13,14] Here the average switching behavior of the dots under the laser spot, an elliptical area with short axis length of 5 μm, is measured and magnetic fields of up to 400 Oe, oriented parallel to the array edge as shown in Fig. 1, were applied. The uniformity of the arrays was confirmed by MOKE measurements carried out at several positions across the array. For example, for the array in Fig. 1(c) the hysteresis loops measured across the 30 μm central region of the array were almost identical, with constant remanent magnetization and only a small decrease in the switching field from 65 Oe at the center to 60 Oe at the edge.

The switching behavior as a function of dot separation was investigated for dot arrays with $h=16$ nm and four different dot sizes, $d=44$, 50, 61, and 66 nm [Fig. 2(a)]. The remanence of the loops is relatively high, with M_R/M_S close to 1, indicating a preference for in-plane magnetization. At large separations, greater than about 50 nm, double switching in the hysteresis loop is observed indicating switching via the vortex state shown schematically with a typical hysteresis loop in Fig. 2(b).[15,16] Here the vortex is nucleated at the edge of the dot at the nucleation field, H_n, and annihilates, again at the dot edge, at the annihilation field, H_a. As the dot separation decreases, there is a change to single switching indicating collective rotation of the magnetic spins during magnetization reversal, as shown schematically with a typical hysteresis loop in Fig. 2(c). It appears that the single switching has been stabilized by magnetic stray field interactions between the dots. In general, the stray field interactions increase as the ratio of dot separation to dot diameter decreases. In addition, switching into the vortex state

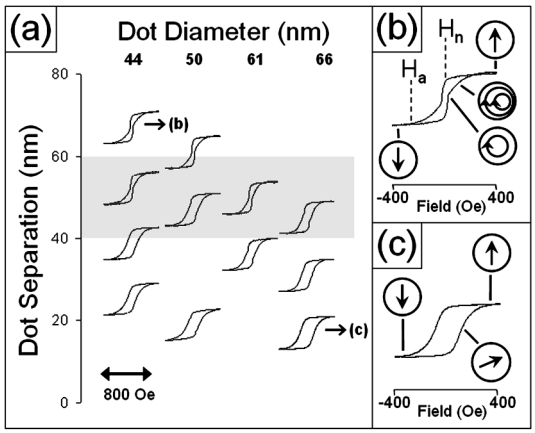

FIG. 2. (a) MOKE hysteresis loops for nickel dot arrays with $h=16$ nm, and various dot diameters and separations. The shaded area highlights the region between 40 and 60 nm where the transition from double to single switching occurs. Typical hysteresis loops with schematic diagrams showing (b) double switching via the vortex state, where H_n and H_a are the vortex nucleation and annihilation fields, respectively, and (c) single switching of collective spins.

becomes more favorable as the dot size increases. The combination of the effect of interdot stray field interactions and dot size results in the transition from double (vortex) to single (collective) switching at a dot separation between 40 and 60 nm, indicated by the shaded area in Fig. 2(a).

In order to visualize the effect of the magnetic stray field interactions, we carried out micromagnetic simulations. The simulations were performed using the OOMMF package (http://math.nist.gov/oommf/) with $d=50$ nm, $h=16$ nm, and a simulation cell size of 2 nm. The saturation moment, M_S, of our nickel films was measured with a vibrating sample magnetometer to be 260×10^3 A/m. This is lower than the value of 485×10^3 A/m for pure nickel which is likely to be a result of the codeposition of impurities into the films during electrodeposition.[7] In order to obtain nucleation of a vortex in a single dot (inset in Fig. 3), the exchange constant, A, was reduced to a value of 5.5×10^{-13} J/m, which is almost 20 times smaller than that for pure nickel. This reduction in the exchange constant is again likely to be a result of impurities introduced during electrodeposition which reduce the

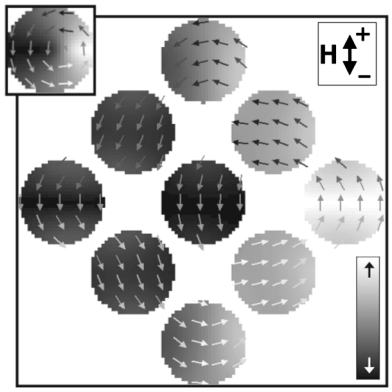

FIG. 3. Snap shot of a micromagnetic simulation showing flux closure through a dot array resulting in single switching in all but the dot farthest to the right. Parameters employed: $d=50$ nm, $h=16$ nm, simulation cell size $=2$ nm, $M_S=260\times10^3$ A/m, and $A=5.5\times10^{-13}$ J/m. The magnetic spins were saturated with a field, H, in the positive direction which was then reduced to zero. The inset shows the vortex state which forms in an isolated dot.

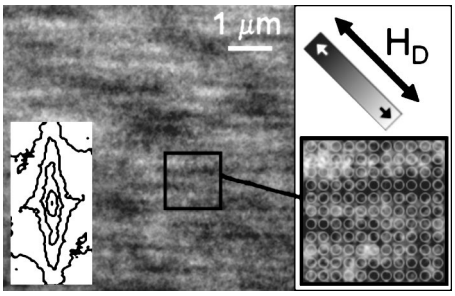

FIG. 4. PEEM image showing bands of contrast in a nickel dot array with $d=95$ nm, $s=18$ nm, and $h=40$ nm. The direction of the demagnetizing field, H_D, which is the same as the magnetization sensitivity direction, is indicated by the double-headed arrow. The contour plot is the Fourier transform of the image, confirming the directionality. The expanded section of the image is overlayed with a schematic of the dot array for comparison, showing that the bands are about two dots wide.

effective exchange interaction. It should also be noted that defects in the nickel dots, both at the surface [e.g., edge defects seen in Fig. 1(c)] and in the volume, will pin magnetic spins and favor vortex nucleation[17] so that it is likely that the reduced exchanged constant required for the simulation is smaller than the actual value for the electroplated nickel system. The low A and M_S could also explain the gradual annihilation of the vortex, which appears as the gradual slope before H_n as seen in Fig. 2(b), rather than the sharp jump in the hysteresis curve seen in Refs. 15 and 16. The magnetic switching in a 3×3 array of 50 nm dots was then simulated and a snapshot of the simulation is shown in Fig. 3. The stray field interaction between the dots favors the collective rotation of the magnetic spins because, rather than forming a vortex in each individual dot (Fig. 3 inset), the flux closure can occur through a series of dots to minimize the magnetostatic energy.

We observed further evidence of the stray field interactions in PEEM magnetic images of the nickel dot arrays. The imaging was carried out on nickel dot arrays with $h=40$ nm, dot sizes $d=95$, 78, and 65 nm and almost constant dot separation, $s=18$, 21, and 20 nm, respectively, at the SIM beamline,[18] Swiss Light Source with an Elmitec PEEM. The arrays were demagnetized by rotating the sample about an in-plane axis in a dc magnetic field, while reducing the field from 3000 Oe down to zero and, employing x-ray magnetic circular dichroism (XMCD), the magnetic domains were imaged by tuning the x-ray energy to the Ni L_3 edge. Dividing two images taken with left and right circular polarized light leads to an XMCD image where the intensity is a measure of the angle between the magnetization and the circular x-ray polarization vector, which we refer to as the magnetization sensitivity direction.[19] Therefore ferromagnetic domains with magnetization parallel or antiparallel to the polarization vector appear black or white in the XMCD image and domains with magnetization perpendicular to the polarization vector will have an intermediate grey contrast. While the dot separation is below the resolution of the PEEM any ordering of the magnetic spins can be observed in the XMCD image, and horizontally running bands of contrast are seen (see Fig. 4). The bands are about two dots wide as seen in the expanded section in Fig. 4, where for comparison a schematic of the dot array is overlayed. The directionality can be explained by the interdot stray field interactions resulting in chains of coupled dots; either single domain dots as seen in the micromagnetic simulation in Fig. 3 or single domain dots interspersed with chains of vortices as the dot diameter and height increases.[16] The fact that this ordering is preferentially horizontal rather than vertical may be due to slight asymmetry in the dot array geometry or because the demagnetizing field, H_D, is experimentally not exactly along the array diagonal.

In conclusion, we have employed XIL to fabricate nanoscale magnetic dot arrays with periods down to 71 nm and uniform over 40 μm, and have observed the effect of stray field interactions on their magnetic behavior. Using XIL it should be possible to produce arrays with areas reaching over several millimeters and even larger areas can be envisaged with implementation of a stepper and multiple exposures. The theoretical minimum period achievable is half the radiation wavelength. We employ an EUV wavelength of 13 nm resulting in a theoretical minimum period of 6.5 nm, suitable for future high density magnetic storage media and devices. Thus the potential of XIL for high resolution and high throughput fabrication of nanoscale magnetic dot arrays will prove to be important for both fundamental scientific research and industrial development, providing essential information about magnetic switching and stray field interactions at the nanoscale.

The authors would like to thank Fredy Glaus, Andrew Podlesnyak, Roger Bischofberger, Konrad Vogelsang, and Michael Horisberger for their support with sample fabrication and measurement. Part of this work was performed at the SLS, Paul Scherrer Institut, Villigen, Switzerland.

[1] P. R. Krauss and S. Y. Chou, Appl. Phys. Lett. **71**, 3174 (1997).
[2] R. M. H. New, R. F. W. Pease, and R. L. White, J. Vac. Sci. Technol. B **12**, 3196 (1994).
[3] J. Moritz, L. Buda, B. Dieny, J. P. Nozieres, R. J. M. van de Veerdonk, T. M. Crawford, and D. Weller, Appl. Phys. Lett. **84**, 1519 (2004).
[4] R. P. Cowburn, J. Appl. Phys. **93**, 9310 (2003).
[5] H. H. Solak, C. David, J. Gobrecht, V. Golovkina, F. Cerrina, S. O. Kim, and P. F. Nealey, Microelectron. J. **67–68**, 56 (2003).
[6] S. O. Kim, H. H. Solak, M. P. Stoykovich, N. J. Ferrier, J. J. de Pablo, and P. F. Nealey, Nature (London) **424**, 411 (2003).
[7] C. A. Ross, M. Hwang, M. Shima, J. Y. Cheng, M. Farhoud, T. A. Sava, H. I. Smith, W. Schwarzacher, F. M. Ross, M. Redjdal, and F. B. Humphrey, Phys. Rev. B **65**, 144417 (2002).
[8] J. Y. Cheng, C. A. Ross, E. L. Thomas, H. I. Smith, and G. J. Vancso, Appl. Phys. Lett. **81**, 3657 (2002).
[9] J. Y. Cheng, C. A. Ross, E. L. Thomas, H. I. Smith, R. G. H. Lammertink, and G. J. Vancso, IEEE Trans. Magn. **38**, 2541 (2002).
[10] S. Sun, C. B. Murray, D. Weller, L. Folks, and A. Moser, Science **287**, 1989 (2000).
[11] M. Albrecht, C. T. Rettner, A. Moser, M. E. Best, and B. D. Terris, Appl. Phys. Lett. **81**, 2875 (2002).
[12] L. J. Heyderman, H. Schift, C. David, B. Ketterer, M. Auf der Maur, and J. Gobrecht, Microelectron. J. **57–58**, 375 (2001).
[13] R. P. Cowburn, D. K. Koltsov, A. O. Adeyeye, and M. E. Welland, Appl. Phys. Lett. **73**, 3947 (1998).
[14] D. A. Allwood, Gang-Xiong, M. D. Cooke, and R. P. Cowburn, J. Phys. D **36**, 2175 (2003).
[15] R. P. Cowburn, D. K. Koltsov, A. O. Adeyeye, M. E. Welland, and D. M. Tricker, Phys. Rev. Lett. **83**, 1042 (1999).
[16] M. Natali, I. L. Prejbeanu, A. Lebib, L. D. Buda, K. Ounadjela, and Y. Chen, Phys. Rev. Lett. **88**, 157203 (2002).
[17] K. J. Kirk, M. R. Scheinfein, J. N. Chapman, S. McVitie, M. F. Gillies, B. R. Ward, and J. G. Tennant, J. Phys. D **34**, 160 (2001).
[18] C. Quitmann, U. Flechsig, L. Patthey, T. Schmidt, G. Ingold, M. Howells, M. Janousch, and R. Abela, Surf. Sci. **480**, 173 (2001).
[19] A. Scholl, H. Ohldag, F. Nolting, J. Stohr, and H. A. Padmore, Rev. Sci. Instrum. **73**, 1362 (2002).